PREPARATION AND CHARACTERISATION OF BISMUTH BASED MATERIALS FOR SOFC APPLICATIONS

Presented in Partial fulfillment of the Requirements for degree of

Master of Science

By Saidatta Naik and Omkar Naik

Under the supervision of

Dr. Bholanath Pahari

UGC-Assistant Professor

School of Physical and Applied Sciences

Goa University

18 MAY 2022

Acknowledgements

We would like to express our deep gratitude and respect to our guide, **Dr. Bholanath Pahari** for his keen interest and valuable guidance, strong motivation and constant encouragement during the course of work. We also thank him for his great patience, constructive criticism and useful suggestions apart from invaluable guidance.

We are also grateful to **Dr. Sudhir Cherukulappurath,** Programme Director of Physics Discipline for his encouragement.

We would also like to thank, **Dr. Anup Bera,** BARC, Mumbai for impedance measurements, **Mr. Santoshkumar Bandaru and Miss. Diksha Karmalkar** PhD students of Physics Discipline, Goa University for their help throughout various stages of our project.

We are also thankful to all the staff members of Goa University, physics dept for their support and encouragement.

Last but not the least; we would like to thank our parents for their moral support.

-Omkar Durgadas Naik **-Saidatta Sanjay Naik**

Contents

Abstract

Chapter 1: Introduction **6-16**

1.1 Fuel cell

1.2 Solid-oxide Fuel Cells (SOFC)

1.2.1 History

1.2.2 Advantages and Disadvantages

1.2.3 Working

1.3 Components of SOFC

1.3.1 Anodes (fuel electrode)

1.3.2 Cathode (air electrode)

1.3.3 Solid electrolyte

1.4 Oxide ion conductor

1.5 Pure bismuth oxide (Bi_2O_3)

1.6 Motivation

Chapter 2: Methodology and characterization **17-33**

2.1 Sample Fabrication of Copper Bismuth Oxide

2.1.2 Method

2.1.2 Chemical Reaction and Balancing

2.1.3 Stoichiometric Calculations

2.2 Sample Fabrication of Bismuth Vanadium Oxide

2.2.2 Method

2.2.2 Chemical Reaction and Balancing

2.2.3 Stoichiometric Calculations

2.3 Characterization of materials

2.3.1 X-Ray Diffraction

2.3.2 UV –Visible spectroscopy

2.3.3 Electrochemical impedance technique

Chapter 3: Results and Discussion **34-46**

3.1 Phase identification using powder x-ray diffraction method

3.2 Energy band gap determination using Uv-Vis Spectroscopy

3.3 Conductivity measurements using impedance spectroscopy

3.3.1 DC Conductivity of CBO

3.3.2 AC Conductivity of BVO

Chapter 4: Conclusion and Future Scope **47-48**

References **49-52**

Abstract

‘Why we should be so concerned about Fuel Cells?’ is a question similar to ‘why we should be so concerned about changing climate or extinction of non-renewable resources?’

The current energy supply systems are mainly based on the combustion of fossil fuels which can cause many environmental problems like air pollution, acid gas emissions, and the emission of greenhouse gases, thus one of the biggest challenges today is to deal both conservation of energy resources and decrease of CO_2 emission. This growing concern over the depletion of fossil fuel resources and the unpredictably adverse climatic conditions has driven us to shift towards renewable energy resources. This however requires mature energy storage and conversion systems. Energy is a lifeblood of global economy. Dawn of this millennium witnesses or triumphal technological march centred on fuel cells. The goal is development, the tool is technology and the path is science. Few technologies have the potential to change the world for better as the fuel cell, which offers a potentially non-polluting and a renewable way to generate electricity. Fuel cells are efficient, clean, safe and reliable. They attract increasing commercial interest for both automotive and stationary power generation [4]. Fuel cells are one of the promising energy conversion and storage technologies that could solve some of the environmental issues, while simultaneously curbing the consumption of resources [1]. They are proposed as promising alternative for large scale generation of electricity, with minimal undesirable chemical, thermal and acoustic emissions [2].

CHAPTER 1

Introduction

1.1 Fuel cells

Fuel cells are electrochemical devices that converts chemical energy to electrical energy. It consists of electrolyte, an ion containing solution, and two electrodes: cathode where reduction of oxygen ion takes place and anode where oxidation of fuel takes place. In this process production of energy takes place and the only byproducts are heat, carbon dioxide and water and thus it doesn't have side effects on environment. If we try to compare between fuel cells and batteries, we see that a battery is an energy storage device that stores its fuel internally and it can supply only a fixed amount of energy but in a fuel cell, reactants are supplied externally, and thus it has no fixed capacity. Therefore, a fuel cell is capable of generating electricity as long as fuels are supplied. Fuel cells can efficiently convert nearly 80% of the chemical energy of the fuel cell into electricity. Advantages of fuel cells are that they can be constructed in modular form. Another advantage of using a fuel cell is that it is fuel flexible. It can accept wide variety of fuels, including natural gas, coal gas, gaseous fuels from biomass and liquid fuels etc. although some fuel may require reprocessing and purification. A single cell normally produces a voltage around of 1.0 volts. To obtain higher voltages the cells have to be connected in series to form a stack. The heat rejected in the process can be used for different on-site thermal consumption. Fuel cells can be classified depending on the type of the electrolyte they incorporate, but much of the interest is focused on commonly used following four types of fuel cells: **solid oxide**, **proton exchange membrane**, **molten carbonate**, and **alkaline fuel cells** [3]. Electrolytes and fuels for some of the fuel cells are as tabulated below.

Type	Operating temperature (°C)	Fuel	Electrolyte	Mobile ion
PEM: Polymer electrolyte membrane	70-110	H_2 , CH_3OH	Sulphonated polymers (Nafions)	$(H_2O)_nH^+$
AFC: Alkali fuel cell	100-250	H_2	Aqueous KOH	OH^-
MCFC: Molten carbonate fuel cell	500-700	Hydrocarbons, CO	$(Na,K)_2CO_3$	CO_3^{2-}
SOFC: Solid oxide fuel cell	700-1000	Hydrocarbons, CO,H_2	$(Zr,Y)O_{2-\delta}$	O^{2-}

Table 1: Fuel cell types and their features [16]

1.2 Solid-oxide Fuel Cells (SOFC)

Solid Oxide Fuel Cell's (SOFC's) are cells that utilizes solid ceramic as electrolyte and operates at high temperatures typically between 973-1273K, where in fuel (H_2) and oxidants (O_2 in air) are constantly feed to electrodes and the by-product is water. SOFC's are called SOFC's because they use solid ceramic electrolytes. The high operating temperatures allows internal reforming, promotes rapid catalysis with no precious metals and co-generation of both electricity and high-quality heat at user site. Over these advantages, high temperatures impose restrictions by reducing the performance of fuel cell over a period of time and affects in deterioration of material properties and interfacial reactions between other fuel cell components.

1.2.1 History

SOFC's originated at the end of 19^{th} century by the discovery of a device, named Nernst mass consisting of yttria-stabilized zirconia (YSZ), devised by Nernst glower. In 1937, Emil Baur and H Preis were successful in operation of first ceramic fuel cell at 1,273 K using coke as fuel and magnetite as oxidant.

1.2.2 Advantages and disadvantages

In general, fuel cells are multilayered ceramic system operating at high temperatures using gaseous fuel and oxidants. These characteristics offers large number of advantages over other fuel cells and generators. Also, there are number of limitations that leads to its slow development. The merits and demerits are discussed below.

SOFC's advantages are they can be modular, operates quietly and are vibration free, can be distributed to eliminate the need of transmission lines. They have simpler design compared to fuel cells with liquid electrolyte, has higher; efficiency and power density. The high operating temperatures reduces activation polarization by enabling high reactant activity, facilitating faster electrode kinetics hence, advantageous as precious platinum electrocatalysts are not required and electrode cannot be poisoned by carbon monoxide. Therefore, there is no requirement of expensive catalysts such as platinum and Ruthenium. Moreover, since the temperatures are sufficiently elevated, so the performance degradation is not due to kinetics but due to ohmic losses (charge transport across components and component interface). SOFC's do not contain any noble metals that could be an issue in availability and high scale manufacturing. Liquid electrolyte fuel cells demand for electrolyte management (electrolyte loss and electrode corrosion), but in SOFC's such problem is not faced. It has low emissions as it converts carbon monoxide to carbon dioxide under high operating temperatures. Other benefits include; low dependence on oil consumption and increasing country's accessibility of electricity, thus securing energy; low operating and maintenance cost; constant power production and allows fuel selection (H_2 can be extracted from natural gas, propane, methanol or diesel fuel).

At 1,273 K, SOFC's are most fuel efficient but, these high temperatures offer a larger number of disadvantages. It decreases the lifetime of the cell and there by increases the cost of the components greatly, as expensive ceramics are used for interconnectors and expensive high temperature alloys are use to house the cell. This drastically increases its cost-to-performance ratio. Therefore, large scale research is going on in reduction of significate operating temperatures of SOFC's. The reduction in temperature will allow use of cheaper interconnectors such as ferric steels without protective coating of lanthanum chromate ($LaCrO_3$) and structural components such as stainless steel. Additionally, it will increase the lifetime of the system by reduction of thermal stress in active ceramic structures. The cell performance is sensitive to operating temperature of SOFC's and requires a significant start-up time as it is seen that 10% drop in temperature results in 12%

drop in cell performance (increase in internal resistance to flow of O_2 ions). Other disadvantages are; high electrolyte resistivity and electrode polarization (change in electrode potential during electrolysis), formation of low conductive phase due to solid state reaction at cathode-electrolyte interface etc. Evolution of compact cell design and improvement in preparation and homogeneity of electrolyte material should be also considered.

1.2.3 Working

A SOFC unit consists of two electrodes namely, cathode and anode, and electrolyte. The fuel (usually Hydrogen H_2 or Methane CH_4) is supplied to anode and oxidant (O_2) is supplied to cathode. The cathode is feed by oxidant or air and transports oxygen ions (O^{2-}) to the electrolyte by accepting electrons from the external circuit. On the other hand, anode receives fuel (H_2 or CH_4) where it reacts with oxide ions from the electrolyte and releases electrons into the external circuit, thus completing the circuit. Thus, the main function of electrolyte is to transport ions between the two electrodes and maintain overall electrical charge balance.

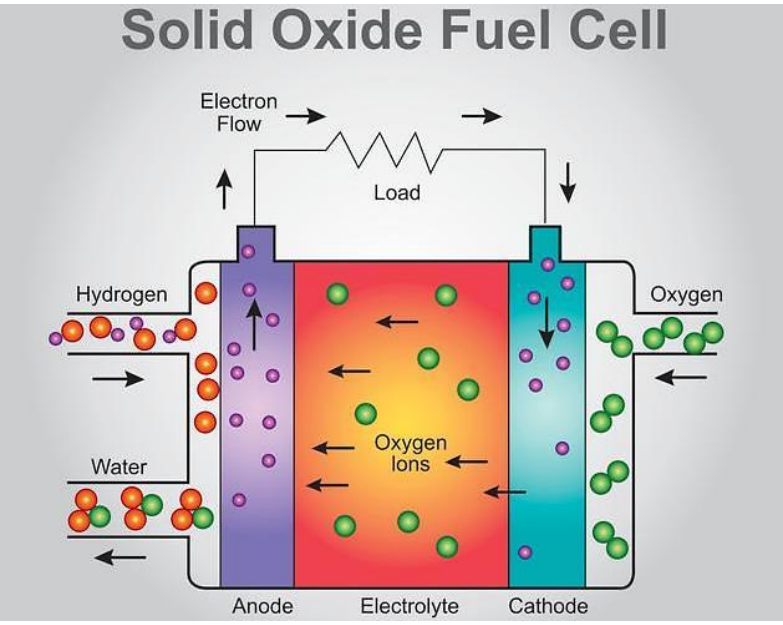

Fig. 1: working of solid oxide fuel cell [22].

1.3 Components of SOFC

Solid oxide fuel cell essentially consists of two porous electrodes separated by a dense, oxygen ion conducting electrolyte. Electrodes in fuel cell are a place where the redox processes take place.

The fuel cell electrodes in the SOFC have the following properties:

1. High electronic conductivity.
2. Chemical and dimensional stability in environments encountered during cell operation and during fabrication of interconnection, electrolyte and fuel electrode layers.
3. Thermal expansion matches with other cell components.
4. Compatibility and minimum reactivity with the electrolyte and the interconnection with which air electrode comes into contact.
5. Compatibility and minimum reactivity with the electrolyte and the interconnection with which air electrode comes into contact.

1.3.1 Anodes (fuel electrode)

The main function of a SOFC anode is to provide electrochemically active sites for the oxidation of the fuel gas molecules and to transport electrons from the site of oxidation to connecting cell components. They thus provide pathways for the fuel to reach the reaction sites and for the reactants to diffuse away from the reaction sites.

The early designs of SOFC considered noble metals such as palladium, silver, platinum and gold and transition metals such as manganese, iron, cobalt, nickel and copper suitable materials for anode. But because of it

Anodes (fuel electrode) are high catalytic activity and redox stability, Ni was chosen as the best choice. However, the pure metal has a strong tendency towards grain growth at elevated temperatures and a significantly different thermal expansion coefficient than commonly used electrolyte materials.

Therefore, nickel is combined with a ceramic compound, such as zirconia or ceria, forming three interconnected frameworks of metal, ceramic and pores. This cermet becomes a good metallic conductor for nickel. The ceramic network not only provides structural integrity and hinders the trapped nickel particles from excessive grain growth but also provides a pathway for oxygen ions, effectively extending the triple phase boundary from the flat electrolyte interface into the anode structure. [20]

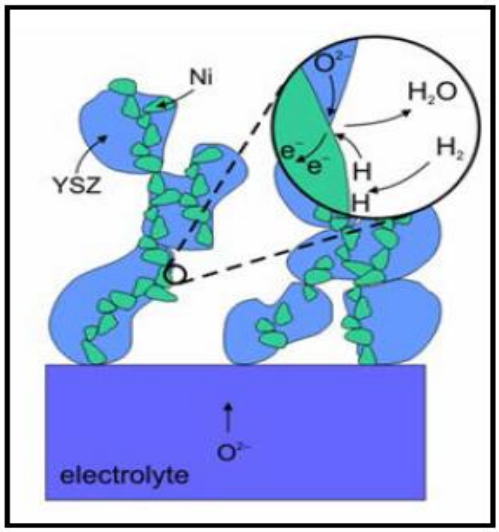

Fig. 2: Oxidation reaction on the surface of an anode made of Ni-YSZ [22].

1.3.2 Cathode (air electrode)

Cathode operates in an oxidizing environment of air or oxygen at 1000°C and participates in the oxygen reduction reaction, which determines the efficiency of the fuel cell and hence plays an important role in the fuel cell [21, 22].Also the highly oxidizing environment of cathode, eliminates the possibility to use cheap base metals [22].Therefore, the choice of cathode materials is rather limited. Although noble metals such as Pt are considered suitable, but their prohibitive costs for SOFC application at higher temperatures compels one to look for better alternatives.

Usually $La_{1-x}Sr_xMnO_{3-x/2}$ (LSM) is used for the cathode when YSZ is used as the electrolyte, because their thermal expansion coefficients match well. Also the mixed ion conductors like $La_{1-x}Sr_xCoO_{3-\delta}$ (LSC) based cathodes are considered. Apart from high electronic and ionic conductivity, MIECs are also feasible for use at low temperatures. This is because of its high ionic conductivity which provides a second pathway for oxygen ions and hence increases its activity. But these materials react with YSZ, thus either ceria-based electrolytes or protective layers of ceria or LSGM on YSZ electrolytes should be used. [20].

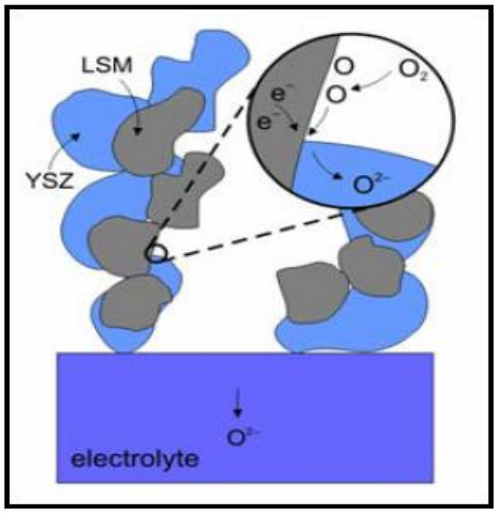

Fig. 3: Reduction reaction on the surface of a cathode made of LSM-YSZ [22].

Table 2: Conductivities of several well-known cathode materials [38]

Cathode	Temperature (^{0}C)	Conductivity (Scm^{-1})
$La_{0.6}Sr_{0.4}CoO_3$	800	1600
$La_{-0.8}Sr_{0.2}Co_{0.2}Fe_{0.8}O_3$	600	1050
$La_{-0.8}Sr_{0.2}Co_{0.2}Mn_{0.2}O_3$	500	1400
$Pr_{0.7}Sr_{0.3}Co_{0.9}Fe_{0.1}O_3$	700	1236

1.3.3 Solid electrolyte

The solid electrolyte is the central component that determines the operational characteristics of the fuel cell system, namely the working temperature. Designing new electrolytes includes manipulation of ionic defects concentration and mobility [6]. The general criteria for the quality of a solid electrolyte material to be used in a SOFC are:

- High ionic conductivity of the range, $\sigma_0 > 10^{-2}$ S/cm at the cell operating temperature

- Negligible electronic conductivity
- Compatibility with the cell components
- Low reactivity
- Compatibility of thermal-expansion coefficients between electrolytes, electrodes.
- Relatively low costs of material and fabrication.

SOFCs are unique with respect to other types of fuel cells for using a ceramic oxide as solid electrolyte. Under operation, the SOFC can use either an oxygen ion-conducting electrolyte or a proton conducting electrolyte, and however most of the current research efforts have been focusing on the SOFC with the oxygen ion-conducting electrolyte [1, 6].

1.4 Oxide ion conductor

They are group of advance ceramic materials, and are most reasonably accepted as the electrolyte in SOFCs. By using oxide ion conductors as the electrolyte, hydrocarbon can be directly used as fuel, and thus, it is possible to use various fuels, which is one of the advantages of SOFCs using oxide ion conductors [7]

In oxygen ion conductors, current flow occurs by the movement of oxide ions through the vacancies. This movement is a result of thermally-activated hopping of the oxygen ions, moving from crystal lattice site to crystal vacant site, with a superimposed drift in the direction of the electric field. The ionic conductivity is consequently strongly temperature dependent, and at high temperatures its value can approach close to 1 S/cm. This type of conduction requires the crystal to contain unoccupied sites equivalent to those occupied by the lattice oxygen ions. Secondly, the energy involved in the process of migration from one site to the unoccupied equivalent site must be small [9]. Therefore, in general the conductivity of any electrolyte can be given as a combined sum of ionic and electronic contributions,

$$\sigma = \sigma_i + \sigma_e = n_i \mu_i (z_i e) + n_e \mu_e e \ \cdots\cdots (1)$$

If the electronic conductivity is negligible and there is only a single mobile ionic species, above equation further reduces to

$$\sigma = \sigma_i = n_i \mu_i (z_i e). \cdots\cdots (2)$$

Where, n_i, μ_i and $(z_i e)$ are respectively the concentration, mobility and charge of the mobile species. Since ions move via defects in the crystal lattice and each type of defect has energies of formation and motion associated with it, we can define this energy as the activation energy E_a and the ionic conductivity can then be given as

$$\sigma = \frac{\sigma_0}{T} e^{-\frac{E_a}{k_B T}} \cdots\cdots (3),$$

Where the pre-exponential term may be expressed as,

$$\sigma_0 = \frac{1}{3k_B} z^2 e^2 n a^2 \omega_0 \cdots\cdots (4).$$

In Eqn. (4) a is the jump distance and ω_0 is the attempt frequency [8].

Oxide ion conductors are also important and technologically exploitable materials used in several types of devices for energy-related and environmental applications. These include oxygen sensors and pumps, dense membranes for oxygen permeation [10].

Well-known oxide ion conductors having good O^{2-} ion conduction property are shown in the plot below.

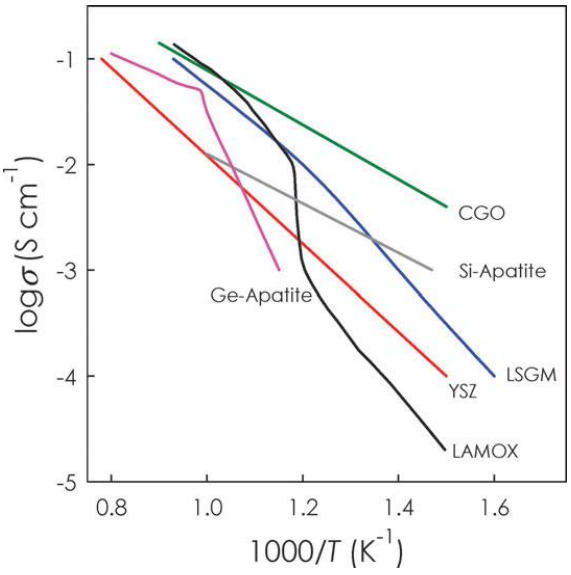

Fig. 4: Total conductivities of several well-known oxide-ion conductors as a function of inverse temperature [5].

Table 3: Conductivities of several well-known oxide ion conductors [5]

Electrolyte	Temperature (°C)	Conductivity (Scm^{-1})
YSZ $(ZrO_2)_{0.92}(Y_2O_3)_{0.08}$	500	$9x10^{-4}$
CGO $Ce_{0.8}Gd_{0.2}O_{1.9}$	500	$2x10^{-2}$
LSGM $La_{0.9}Sr_{0.1}Ga_{0.8}Mg_{0.2}O_{2.85}$	500	$7x10^{-3}$
LAMOX $La_2Mo_2O_9$	500	$5x10^{-4}$
Si-apatite $La_{10}(SiO_4)_6O_3$	500	$5x10^{-3}$
Ge-apatite $La_{10}(GeO_4)_6O_3$	727	$5x10^{-2}$

As can be seen in the plot, most of the oxide ion conductors have high ion conductivity at high temperature (<800 °C). Thus the obstacle in the commercialization of SOFCs is their high operating temperature. It is reasonable to consider that the fuel cell operating temperature mostly depends on the choice of the electrolyte material. Thus the choice of the electrolyte material, conductivity, stability and the availability of suitable techniques for fabrication of thin films become critical issues in consideration of the lower temperature operation. Lowering the operating temperature is advantageous since it can help reduce the cost for operation and materials. Also the cell degradation problems, such as inter-diffusion between cell components, can be mitigated [4]. Currently stabilized zirconia, especially yttria-stabilized zirconia (YSZ) is extensively used as an electrolyte for SOFCs.YSZ is one of the best oxide ion conductors and its high-temperature polymorph has fluorite crystal structure and may be stabilized to room temperature by formation of solid solutions with CaO, Y_2O_3, etc. Stabilized zirconia exhibits high O^{2-}ion conductivity at high temperatures because of the mechanism of solid solution formation which involves the creation of vacant O^{2-}sites in order to preserve electro neutrality [11]. Other O^{2-}ion conductors are Bi_2O_3andZrObased compound. However, compared to Bi_2O_3, solid electrolytes based on ZrO, have relatively low oxide ion conductivity at temperatures below 800 K and require very high sintering temperatures (often higher than 2000 K) [12].

Motivation

In recent publications $CuBi_2O_4$ and $Bi_{-0.913}V_{0.087}O_{1.587}$ are proposed as promising cathode and electrolyte materials, respectively for SOFC application with low operating temperature. In context to we aim to investigate their crystal structure and electrical properties. Also it is necessary for inspecting the chemical stability of the two in contact with each other as cell components.

CHAPTER 2

Methodology and Characterization

2.1 Sample Fabrication of Copper Bismuth Oxide (CBO)

2.1.1 Method

CBO powder was synthesized by a conventional solid state reaction method. Typically, stochiometric amounts of Bi_2O_3 (99.99%) and CuO (99.99%) oxides were mixed uniformly through mechanic mortar and pestle. After drying, the mixture was calcinated at 780°C in air for 36 hours with several intermediate grindings to obtain the CBO cathode powder. Further, $Bi_{0.913}V_{0.087}O_{1.587}$ powder was sintered at 800°C for 12 hours.

2.1.2 Chemical Reaction and Balancing

The reaction is as follows;

$$Bi_2O_3 + CuO \longrightarrow CuBi_2O_4$$

Since, the number of Bi, Cu and O atoms remains same before and after reaction the above equation is balance.

2.1.3 Stoichiometric Calculations

For preparation of 2g of $CuBi_2O_4$ powder, the amount of Bi_2O_3 and CuO was found by stoichiometric calculations.

Elements	Molecular weights in a.m.u.
Bismuth (Bi)	208.98
Copper (Cu)	15.99
Oxygen (O)	63.58

Table 4: Molecular weights of different elements.

$CuBi_2O_4 = [63.54+(2x208.98)+(4x15.99)]\ x$

$CuBi_2O_4 = 545.46\ x$

For 2g of $CuBi_2O_4$

$CuBi_2O_4 = 2g$

$545.46\ x = 2$

$$x = \frac{2}{545.46}$$

$x = 3.66 \times 10^{-3}$

Now, we find the amount of Bi_2O_3 and CuO to prepare 2g of $CuBi_2O_4$ by using the value of x.

$Bi_2O_3\ x = A$

$[(2x208.98)+(3x15.99)]x\ x = A$

$[465.93] \times [3.66 \times 10^{-3}] = A$

$A = 1.7084g$

$CuOx = B$

$[(1x63.54)+(1x15.99)]x\ x = B$

$$[79.53 \text{ x } [3.66\text{x}10^{-3}] = \text{B}$$

$$\text{B} = 0.2916\text{g}$$

$$\text{A} + \text{B} = 2\text{g}$$

$$1.7084 + 0.2916 = 2\text{g}$$

Therefore, 1.7084g of Bi_2O_3 and 0.2916g of CuO to prepare 2g of $CuBi_2O_4$.

2.2 Sample Fabrication of Bismuth Vanadium Oxide ($Bi_{0.913}V_{0.087}O_{1.587}$)

2.2.1 Method

$Bi_{0.913}V_{0.087}O_{1.587}$ powder was synthesized by a conventional solid state reaction method. Typically, stochiometric amounts of Bi_2O_3 (99.99%) and V_2O_5 (99.99%) oxides were mixed uniformly through mechanic mortar and pestle. After drying, the mixture was calcinated at 700, 750, 800°C in air for 36 hours with several intermediate grindings to obtain the $Bi_{0.913}V_{0.087}O_{1.587}$ electrolyte powder. Further, $Bi_{0.913}V_{0.087}O_{1.587}$ powder was sintered at 800°C for 12 hours.

2.2.2 Chemical Reaction and Balancing

The reaction is as follows;

$$Bi_2O_3 + V_2O_5 \longrightarrow Bi_{0.913}V_{0.087}O_{1.587}$$

The balanced reaction is

$$0.913(Bi_2O_3) + 0.087(V_2O_5) \longrightarrow 2(Bi_{0.913}V_{0.087}O_{1.587})$$

Since, the number of Bi, V and O atoms remains same before and after reaction the above equation is balance.

2.2.3 Stoichiometric Calculations

For preparation of 2g of $Bi_{0.913}V_{0.087}O_{1.587}$ powder, the amount of Bi_2O_3 and V_2O_5 was found by stoichiometric calculations.

Elements	Molecular weights in a.m.u.
Bismuth (Bi)	208.98
Vanadium (V)	50.9415
Oxygen (O)	63.58

Table 5: Molecular weights of different elements.

$$2(Bi_{0.913}V_{0.087}O_{1.587}) = 2[(208.98x0.913) + (50.9415x0.087) + (15.99x1.587)]\ x$$

$$2(Bi_{0.913}V_{0.087}O_{1.587}) = 2(220.607)\ x$$

For 2g of $Bi_{0.913}V_{0.087}O_{1.587}$

$$Bi_{0.913}V_{0.087}O_{1.587} = 2g$$

$$2x220.607\ x = 2g$$

$$x = \frac{1}{220.607}$$

$$x = 4.5329\ x10^{-3}$$

Now, we find the amount of Bi_2O_3 and V_2O_5 to prepare 2g of $Bi_{0.913}V_{0.087}O_{1.587}$ by using the value of x.

$$Bi_2O_3\ x = A$$

$$[0.913x(2x208.98)+(3x15.99)]x\ x = A$$

$$\{0.913[465.93]\ x\ [3.66x10^{-3}]\} = A$$

$$A = 1.9283g$$

$$V_2O_5x = B$$

$$[0.087x(2x50.9415)+(5x15.99)]x\ x = B$$

$$\{0.087x[79.53\ x\ [3.66x10^{-3}]\} = B$$

$$B = 0.0717g$$

$$A + B = 2g$$

$$1.9283+0.0717= 1.9999 \cong 2g$$

Therefore, 1.9283g of Bi_2O_3 and 0.0717g of V_2O_5 to prepare 2g of $Bi_{0.913}V_{0.087}O_{1.587}$.

2.3 Characterization of materials

2.3.1 X-Ray Diffraction

X-ray diffraction is a non-destructive analytical technique which reveals information about the crystallographic structure, chemical composition, and physical properties of materials. This technique is based on observing the scattered intensity of an X-ray beam hitting a sample as a function of incident and scattered angle. It is therefore an important experimental technique used to uniquely identify the crystalline phases of the materials and to measure their structural parameters such as lattice constants, grain size, and phase composition [24].

Principle:

Max von Laue discovered that crystalline substances act as three-dimensional diffraction gratings for X-ray wavelengths similar to the spacing of planes in a crystal lattice. That means X-rays can be diffracted from materials which, by definition are crystalline and have regularly repeated atomic structures. Therefore, when certain geometric requirements are met, X-rays scattered from a crystalline solid can constructively interfere, producing a diffracted beam. This geometric condition corresponds to Bragg's law [24].

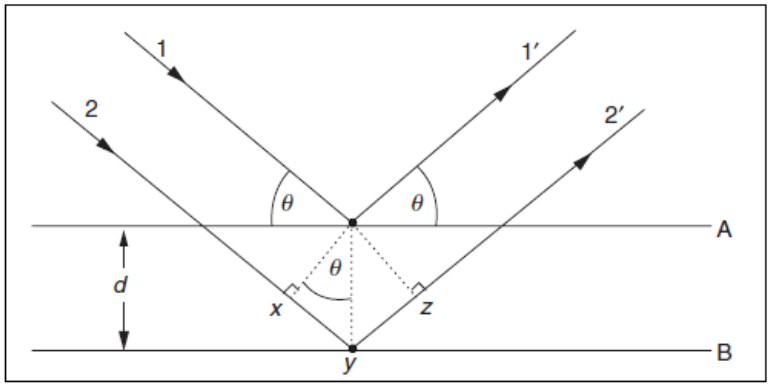

Fig.4: Derivation of Bragg's law [25]

In Bragg's approach to diffraction, crystals are considered to be built in the form of layers or planes and each plane acts as a semi-transparent mirror. Two X-ray beams, 1 and 2 are reflected from adjacent planes, A and B, within the crystal. As can be seen from Fig.1, beam 22' has to travel an extra distance *xyz* compared with beam 11'; and for 1' and 2' to be in-phase, the distance *xyz* must equal a whole number of wavelengths [25].

The relation between perpendicular d-spacing, Bragg angle (θ) and the distance *xy* can be given as

$$xy = yz = d \sin\theta$$

Hence,

$$xyz = 2d \sin\theta$$

However,

$$xyz = n\lambda$$

And therefore,

$$n\lambda = 2d \sin\theta \ldots\ldots (1)$$

Equation (1) is Bragg's law

Therefore, when Bragg's law is satisfied, the reflected beams are in-phase and interfere constructively, however incase of angles other than the Bragg angle, reflected beams are out-of-phase and destructive interference or cancellation occurs. For a given set of planes, several solutions of Bragg's law are usually possible, for n = 1, 2, 3, etc. However, it is customary to set $n=1$ and for situations where, say, n = 2, the d-spacing is instead halved by doubling the number of planes in the set; hence n is kept equal to 1[25].

Conversion of the diffraction peaks to d-spacing allows identification of the material because each material has a set of unique d-spacing. Thus, the typical characteristic peaks provided by

diffraction pattern is unique 'fingerprint' of the minerals present in the sample. Interpretation can be then achieved by comparison d-spacing with standard reference patterns [24].

Working:

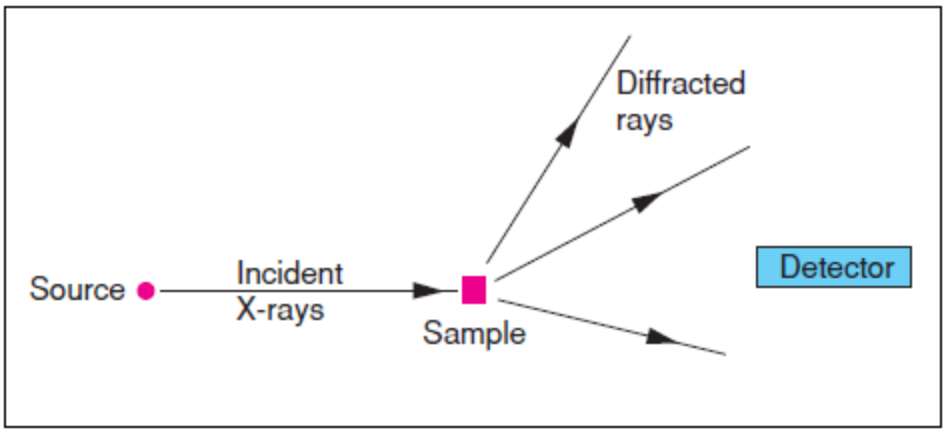

Fig.5: The X-ray diffraction experiment [25]

X-ray diffractometers consist of three basic elements:

a) Radiation-monochromatic or of variable, λ
b) Sample - single crystal, powder or a solid piece.
c) X-ray detector- radiation counter or photographic film.

In a cathode ray tube, filament is heated to emit electrons and these electrons are then accelerated towards a target by applying a voltage (≥10 kV), thus producing X-ray. However, when electrons have sufficient energy to dislodge inner shell electrons of the target material, characteristic X-ray spectra are produced. These spectra consist of several components, the most common being K_α and K_β. But for most diffraction experiments, a monochromatic beam of X-rays is desired and not a continuous spectrum and hence it is necessary to filter out all other wavelengths. These X-rays are then collimated and directed onto the sample. As the sample and detector are rotated, the intensity of the reflected X-rays is recorded. When the geometry of the incident X-rays impinging the sample satisfies Bragg's law, constructive interference occurs and a peak in intensity appears. A detector records and processes this X-ray signal and converts the signal to a count rate, which is then transferred to a device such as a printer or computer monitor [24].

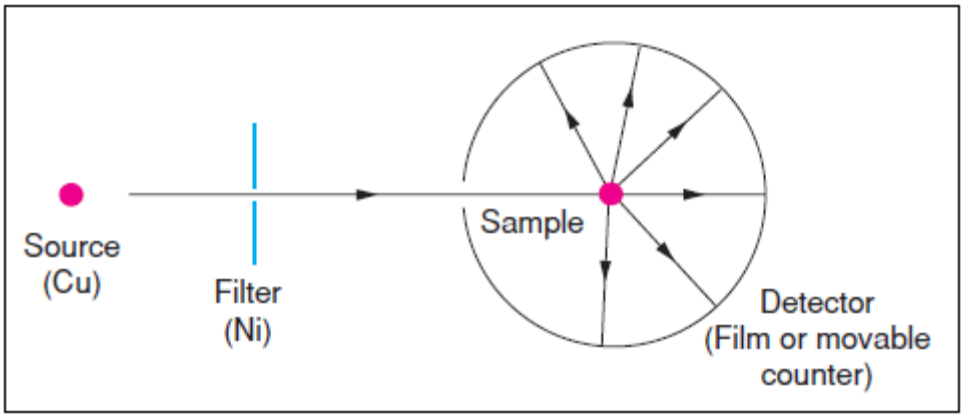

Fig.6: The powder method [25]

Copper is the most common target material with Cu K_α radiation, λ=1.5418Å and Ni foil is a very effective filter for copper target.

In finely powdered sample, crystals are randomly arranged in every possible orientation and various lattice planes are also present in every possible orientation. Therefore, for each set of planes, at least some crystals must be oriented at the Bragg angle, θ, to the incident beam and thus diffraction occurs for these crystals and planes. The diffracted beams may be detected either by surrounding the sample with a strip of photographic film or by using a movable detector [25].

2.3.2 UV –Visible spectroscopy

When a beam of electromagnetic radiation interacts with a material, it can be absorbed, transmitted, scattered or reflected. UV-Visible spectroscopy refers to absorption /reflectance spectroscopy in the ultraviolet-visible spectral region. It is therefore used to measure the intensity of radiation absorbed by the sample in the wavelength range from near-ultraviolet through visible to near infra-red region and is scanned normally from 200 to 800 nm [27].

UV-Visible spectroscopy, as a technique of characterization, deals with the study of electronic transitions between orbitals or bands of atoms, ions or molecules in the gaseous, liquid and solid phase [28].Thus it can be used to find out the nature of transitions of carriers and band gap of a material by investigating measurement of the absorption edge of the material [29].

Principle

UV spectrophotometer principle follows the Beer-Lambert Law which states that transmittance i.e. the intensity of transmitted light (I_T) over the incident intensity (I_0), is dependent on the path length of the light through the sample (l), the absorption cross section (σ) of the sample's transition, and the difference in the population of the initial state (N_1) and final state (N_2),

$$T = \frac{I_T}{I_0} = e^{-\sigma(N_1 - N_2)l} \ldots\ldots (1)$$

This is often written in a form referred to as Beer's Law, equation (2)

$$\mathrm{A} = \varepsilon c l = -\log_{10}\left(\frac{I_T}{I_0}\right)$$

Or,

$$I_T = I_0(10)^{-\varepsilon c l} \ldots\ldots. (2)$$

Where, A is the absorbance, ε is the molar absorptivity coefficient of the material, c is the concentration of the absorbing species, and l is the path length of the light through the sample [26].

The absorbance A can be normalized to the path length l of the light through the material (e.g. the thickness) producing the absorption coefficient α,

$$\alpha(cm^{-1}) = \frac{\ln(10) \times A}{l(cm)}$$

Or,

$$\alpha(cm^{-1}) = \frac{2.303 \times A}{l(cm)}$$

If a beam of photons with hν >E_g falls on a material, there will be some predictable amount of absorption determined by the properties of the material.

The intensity of light transmitted through the sample of thickness, l is given by

$$I_T = I_0 e^{-\alpha l}$$

Near the absorption edge, the absorption coefficient is then expressed as

$$\alpha \sim \left(E_g - h\nu\right)^{\gamma}$$

Where, hν is the photon energy, E_g is the optical gap, γ is a constant which is equal to 1/2 and 3/2 for allowed direct transition and forbidden direct transition whereas it is equal to 2 for indirect transition. The shape of the UV-vis absorption spectrum can distinguish between these transitions [26, 30].

In materials with a large exciton binding energy, absorbed photon will have barely enough energy to create an exciton, but not enough energy to separate the electron and hole. Therefore, in such a case, there is a distinction between optical band gap and electrical band gap (transport gap). The optical band gap is the threshold for photons to be absorbed, whereas the transport gap is the threshold for creating an electron–hole pair that is not bound together. The optical band gap is at lower energy than the transport gap and the difference between the two energy gaps is the binding energy of the exciton. [31].

Working

A spectrophotometer generally consists of four components:

1. Light source which covers the UV-VIS spectrum of interest. In general, a lamp containing a gas such as xenon, or a combination of two different lamps such as tungsten/deuterium is used.
2. An appropriate sample holder is needed to hold the sample.
3. A dispersion element is needed to distribute the light into separate wavelengths. It can be either a quartz prism or a diffraction grating.
4. Finally, the transmitted light intensity is recorded by a suitable detector such as photomultiplier, a multichannel array (e.g. a photodiode array, or PDA), or a charge-coupled device (CCD).

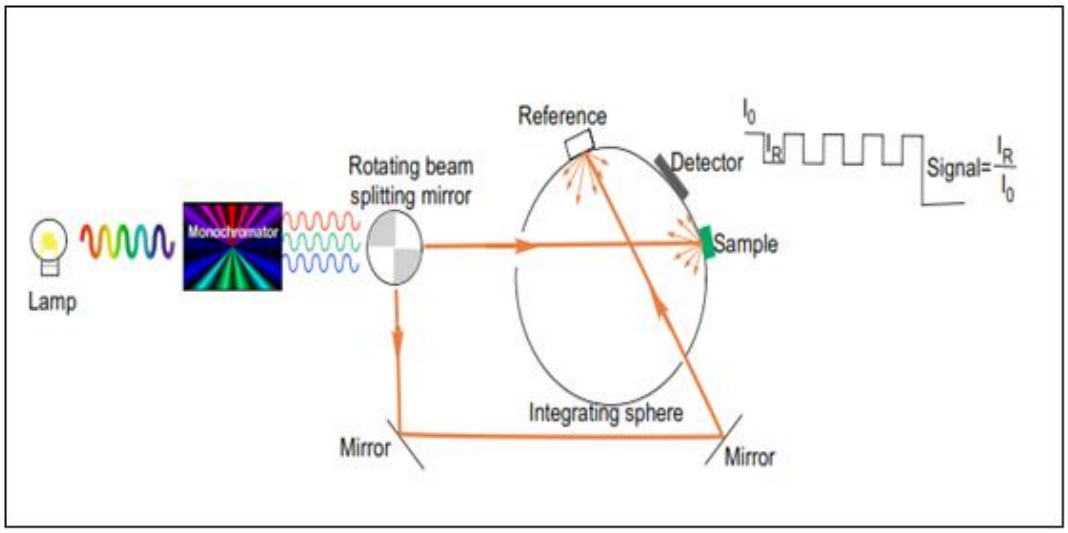

Fig.7: Optical system of a dual-beam reflectance spectrophotometer [26]

The two most commonly used UV-vis configurations are transmission and diffuse reflectance. In general, transmission mode is used for transparent samples. Often these materials are single crystals or thin films supported on transparent glass substrates. Opaque or translucent samples, such as materials supported on metallic substrates or solids made up on small particles or multiple small crystals, cannot be used since they strongly scatter light and therefore in transmission mode the spectrometer would indicate complete absorption across all wavelengths of light. As such, opaque samples must utilize a diffuse reflectance configuration. Both techniques follow the general experimental format:

- Turn on lamp source and allow at least 15 minutes for lamp to warm up
- Place reference sample into the light path. All the absorption spectra and transmission spectra were recorded keeping air as the reference and reflection spectra was taken by keeping Ba_2SO_4 as reference.
- Collect a baseline of the reference sample
- Place working sample into the light path
- Collect transmission/reflection spectrum of working sample
- Calculate the absorption coefficient and convert wavelength from nm to eV
- Fit the spectrum to estimate the band gap and assess whether it is direct or indirect and whether it is forbidden or allowed [26].

2.3.3 Electrochemical impedance technique

Electroceramics are advanced materials made up of constituent components which have different frequency dependences [33]. Generally, the dielectric properties in such materials arise due to inter-grain, intra-grain and electrode processes and it is important to separate these properties in order to unravel the complexities of such material and to have a control over properties [33, 34].This can be achieved using electrochemical impedance technique. Thus EIS is a highly sensitive characterization technique used to establish the electrical response of chemical systems in nondestructive manner [32].

In general ceramic placed between the electrodes can be expressed by Brickwood model which represents a ceramics composed of cubic grains of dimension l_1 and separated by grain boundaries of thickness l_2.

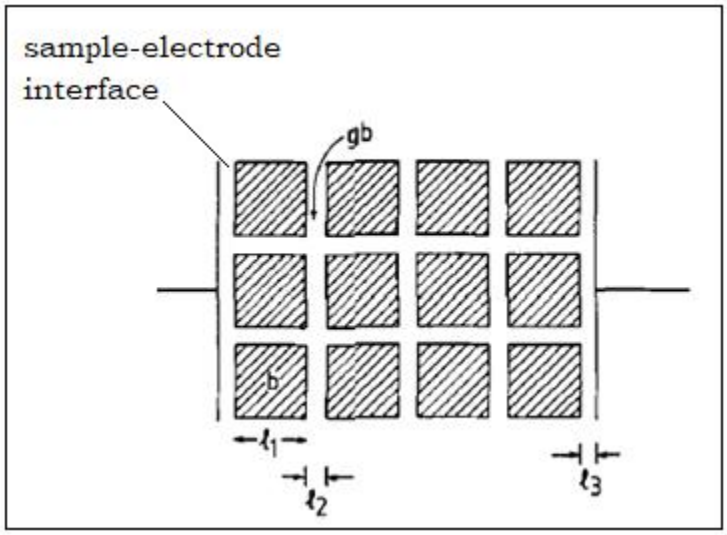

Fig.8: Brickwork model of grain and grain boundary regions in a ceramic placed between metal electrodes [33].

From the above figure, the relation $\frac{C_{gb}}{C_b} = \frac{l1}{l2}$ can be derived.[33]

Principle:

Principle of EIS is based on Faraday's Law to characterize a chemical process in terms of electrical measurements. During Impedance measurement an AC voltage is applied to a sample at different frequencies and the current is measured. The value of measured current will be determined by the mechanisms of reaction taking place within the sample. The reaction mainly involves the formation of new chemical species as result of the movement of ions through the electrolyte. Thus the flow of electric current is a result of ionic movements caused by the applied potential difference [35],

The applied ac is of form given by eq (1)

$$E(t) = E_0 \sin(\omega t) \ldots\ldots (1)$$

In order to circumvent nonlinear response of electrochemical systems EIS technique measures impedance using a small excitation signal. This perturbative ac signal ensures pseudo-linear response which means the current response to a sinusoidal potential will be a sinusoid at the same frequency but shifted in phase as can be seen in the eq (2) [34,35]

$$I(t) = I_0 \sin(\omega t + \theta) \ldots\ldots (2)$$

The impedance can therefore be expressed as

$$Z = \frac{E(t)}{I(t)} = \frac{E_0}{I_0} \frac{\sin(\omega t)}{\sin(\omega t + \theta)} = |Z| \frac{\sin(\omega t)}{\sin(\omega t + \theta)} \ldots\ldots (3)$$

Thus the impedance has a magnitude $|Z|$ and phase θ and the two components of vector Z can be written in the form as given below:-

$$|Z'| = |Z| \cos\theta$$

$$|Z''| = |Z| \sin\theta$$

When ac sinusoidal voltage is applied across a pure resistance of magnitude *R*, the magnitude of impedance is $Z = R$ and the phase $\theta = 0$ for all frequencies. However, in case of a pure capacitance, the impedance is given as $Z = 1/\omega C$ and phase $\theta = 90°$. Thus the impedance is frequency dependent

and as frequency increases impedance decreases [35]. EIS can therefore be used in analysis ceramic samples where different regions are characterized by a resistance and a capacitance, usually placed in parallel and the characteristic time constant of each 'parallel *RC* element' is given by[33]eq(4)

$$\tau = R\mathrm{C}$$

Analysis of the impedance data is carried out using complex plane method. The complex series impedance$Z = Z^{'} - jZ^{"}$, is represented by a plot of real component $Z^{'}$ vs. imaginary component $Z^{"}$.This plot is commonly called as Cole-Cole plot or complex plane plot.

The total impedance Z of the circuit containing one parallel RC component is given by,

$$Z = \frac{R}{1+j\omega CR} = Z' - jZ^{"} \ldots\ldots\ldots (5)$$

Therefore,

$$Z' = \frac{R}{1+(\omega cR)^2} \ldots\ldots (6)$$

And,

$$Z^{"} = \frac{\omega CR^2}{1+(\omega cR)^2} \ldots\ldots (7)$$

Eliminating ω , we get

$$(Z' - {}^{R}/_{2})^2 + (Z^{"} - 0)^2 = (R/2)^2 \ldots\ldots\ldots (8)$$

Eq (8) represent the equation of a circle with center coordinate (R/2, 0) and radius equal to R/2. When we plot, $Z^{"}$ vs. of the co-ordinate at the top of the semi-circular arc, at a particular frequency ω_o is (R/2, R/2). Thus, by substitution of Z' = R/2 and Z" = R/2 in Equations (6) and (7), the relation ω_oRC = 1 is obtained,

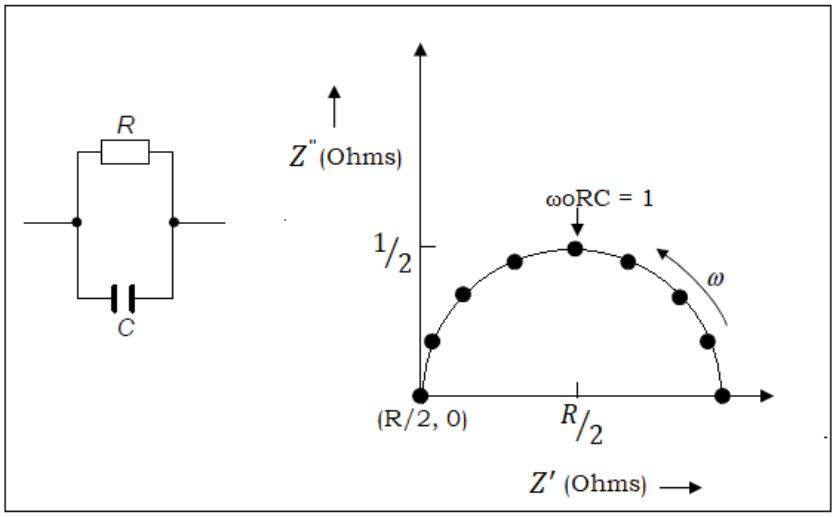

Fig.9: Complex plane impedance Spectrum-Parallel resistance, capacitance [35].

Therefore in frequency domain, different RC elements are separable due to the relation, $\omega_o RC = 1$ where ω_0 is the frequency of maximum loss in impedance spectrum.

In order to account for grain and grain boundary effects, equivalent circuit will now consist of a series collection of two sub-circuits (consisting of a resistor and capacitor connected in parallel).The complex impedance for the equivalent circuit is given by:

$$Z = \frac{1}{\frac{1}{R_g} + j\omega C_g} + \frac{1}{\frac{1}{R_{gb}} + j\omega C_{gb}} = Z' - jZ'' \ldots\ldots (9)$$

Where R_g and C_g are bulk resistance and capacitance respectively and R_{gb} and C_{gb} are grain boundary resistance and capacitance respectively.

Therefore,

$$Z' = \frac{R_g}{1 + (\omega C_g R_g)^2} + \frac{R_{gb}}{1 + (\omega C_{gb} R_{gb})^2}$$

And

$$Z'' = \frac{\omega C_g {R_g}^2}{1 + (\omega C_g R_g)^2} + \frac{\omega C_{gb} {R_{gb}}^2}{1 + (\omega C_{gb} R_{gb})^2}$$

Based on the above equations, the response peaks of the grains and grain boundaries are represented by 1/ (2πRgCg) and 1/ (2πRgbCgb) respectively, and the peak values are proportional to the associated resistance.

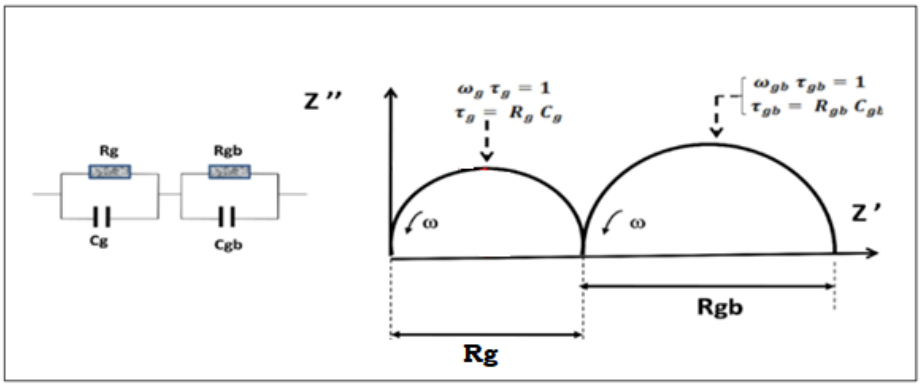

Fig.10: Nyquist plot for equivalent circuit containing two parallel RC elements in series [38]

Working

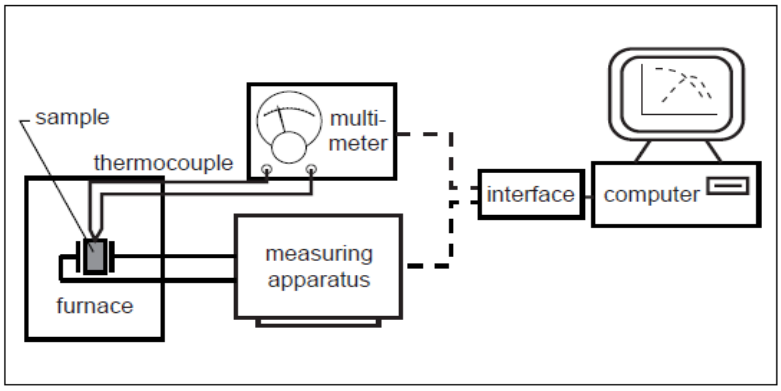

Fig.11: Experimental setup of EIS system set up [36].

In this technique, AC impedance measurements are made over a wide range of frequencies typically from 10^{-2} to 10^{7} Hz and different contributions to the overall response arising from bulk (grains), grain boundaries, and electrodes can be determined [33].

The measuring apparatus is directly connected to the sample and generates the electrical data. Measurements at different temperatures are obtained by placing the sample into a temperature-controllable furnace. A thermocouple is placed near the sample to verify the temperature, read either in terms of induced voltage (millivolts) or temperature. For automated data acquisition, the measuring system can be directly coupled to a computer through the appropriate interface. In case of frequency-domain, the sample's electrical data are recorded by means of frequency response analyzers, impedance analyzers, or high-precision inductance–capacitance–resistance meters.

Once this data is obtained, it can be presented in a form of complex diagrams. Thereafter the parameters of an equivalent circuit are fitted to reproduce the measured impedance spectra. These circuit parameters are then associated with the physical and chemical processes occurring in the material [38]

CHAPTER 3

Results and Discussions

3.1 Phase identification using powder x-ray diffraction method

CBO and BVO systems were prepared by solid state reactions. The phase purity of both the materials were determined by powder X-ray diffraction (XRD). X-ray powder diffraction data was collected for all samples at room temperature in the range of $10° \leq 2\theta \leq 80°$ at the scan speed of 2°/min using monochromatic Cu Kα radiation having 1.54 Å wavelength.

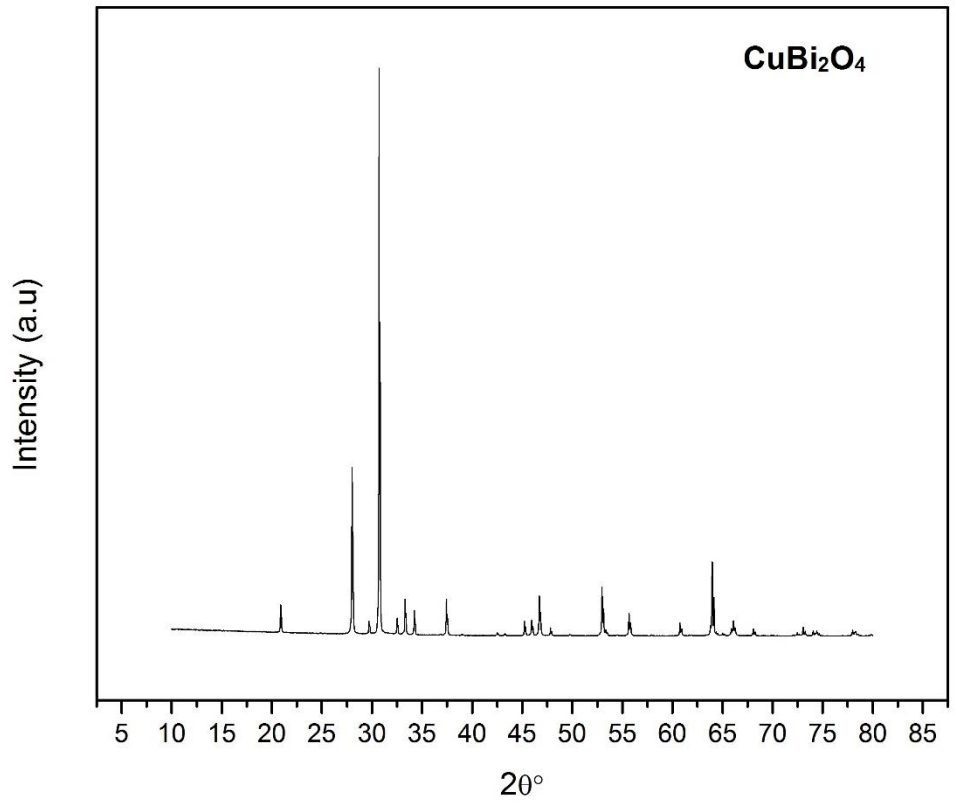

Fig 12.: X-ray diffraction pattern of $CuBi_2O_4$ (CBO)

Fig. 12 shows the XRD pattern of the prepared powder sample. The XRD data was analyzed using CELREF software, which was also used to refine cell parameters from diffraction data by iterative

least squares refinement of initial cell parameters. Results of the XRD data analysis by CELREF are as shown below.

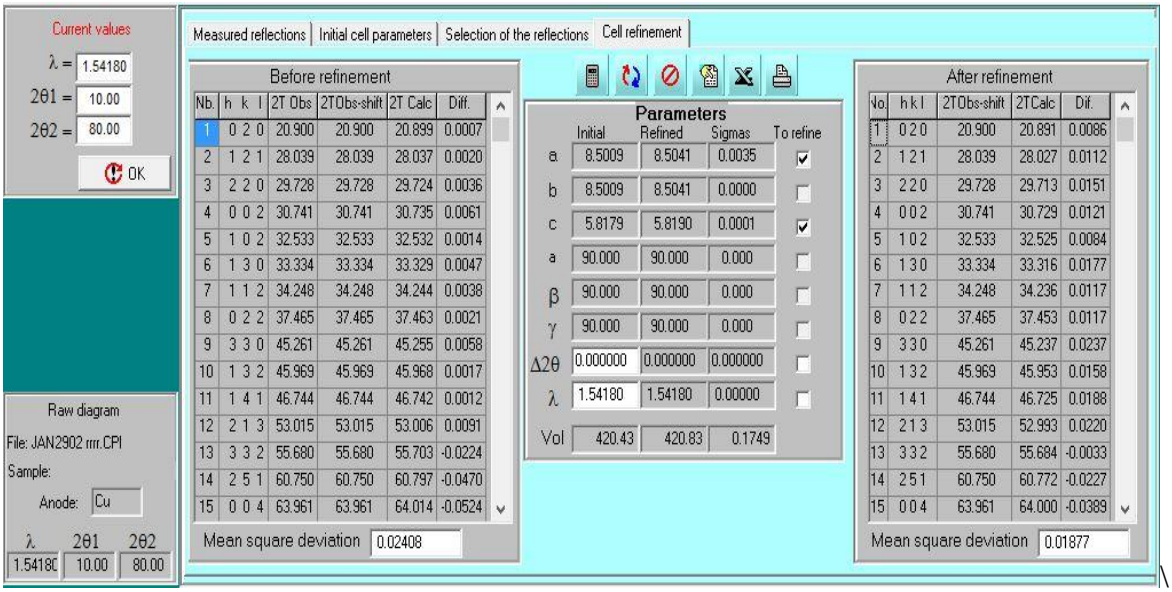

Fig 13 .: XRD data analysis by CELREF for CBO

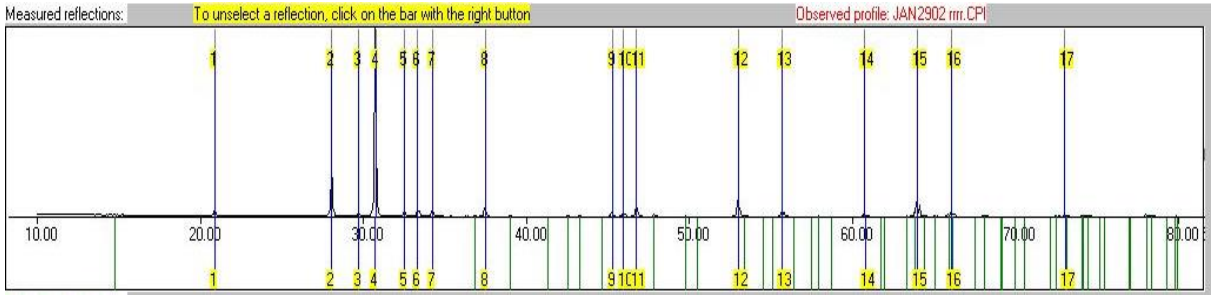

It can be seen that all the diffraction peaks are in good agreement with the calculated Bragg's position. It is also in close agreement with the XRD pattern in the paper N. Li et al. for tetragonal CBO with space group of P4/ncc, and no impurity peaks are observed. These results imply that CBO powder has been synthesized successfully, by solid state reaction method.

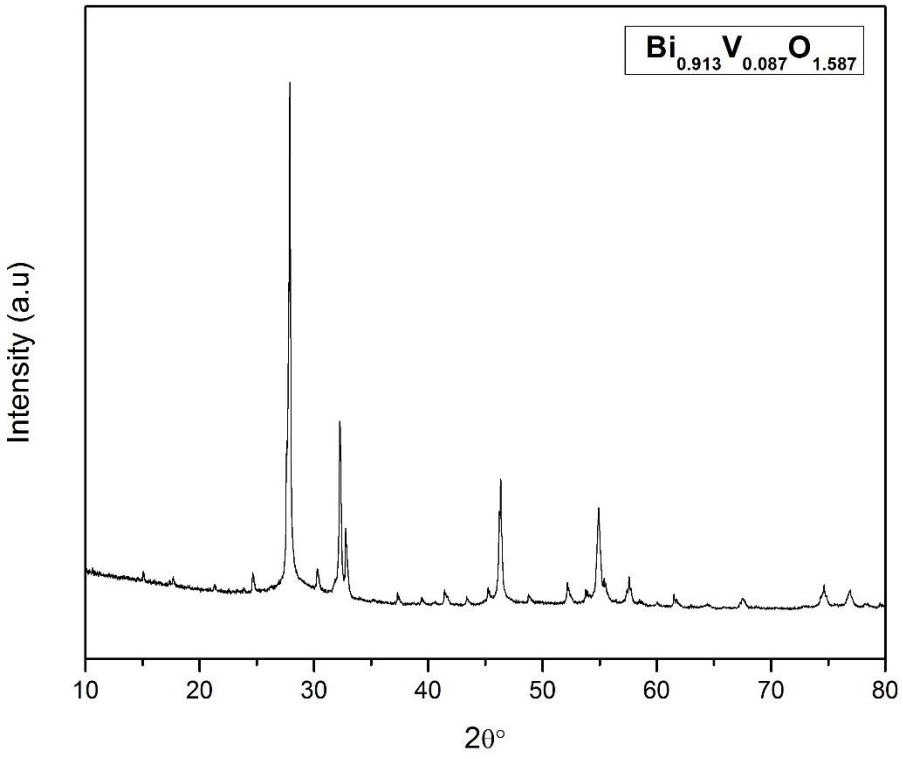

Fig 14.: X-ray diffraction patterns of BVO is as shown in Figure

Fig. 14 shows the XRD pattern of the as prepared $Bi_{0.913}V_{0.087}O_{1.587}$ (BVO) sample, which was synthesized by solid state reaction at 800°C for 24 hours. It can be seen that major peaks of the diffraction pattern are in good agreement with the standard XRD pattern in the reported article. The XRD pattern can be indexed with a cubic unit cell and space group of $Fm\bar{3}m$. However, an extra phase (minor phase) has been observed which has been identified with space group $I23$. The XRD data was analyzed using CELREF software, which was also used to refine cell parameters from diffraction data by iterative least squares refinement of initial cell parameters. Results of the XRD data analysis by CELREF are as shown below.

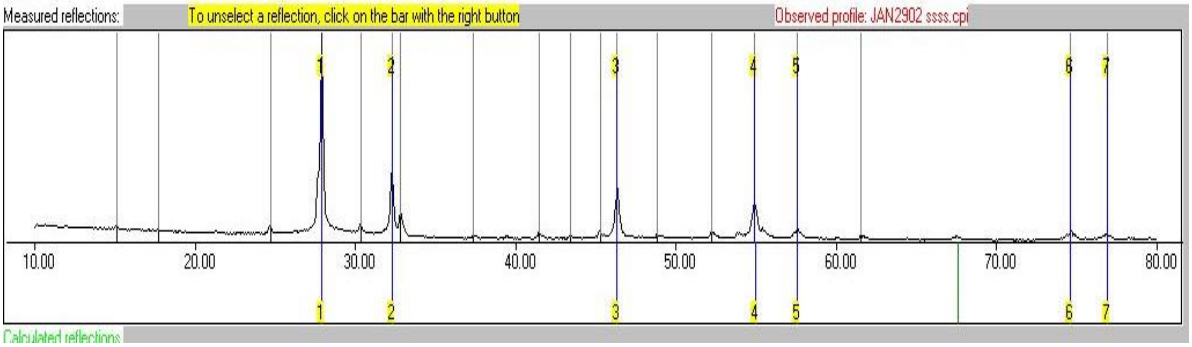

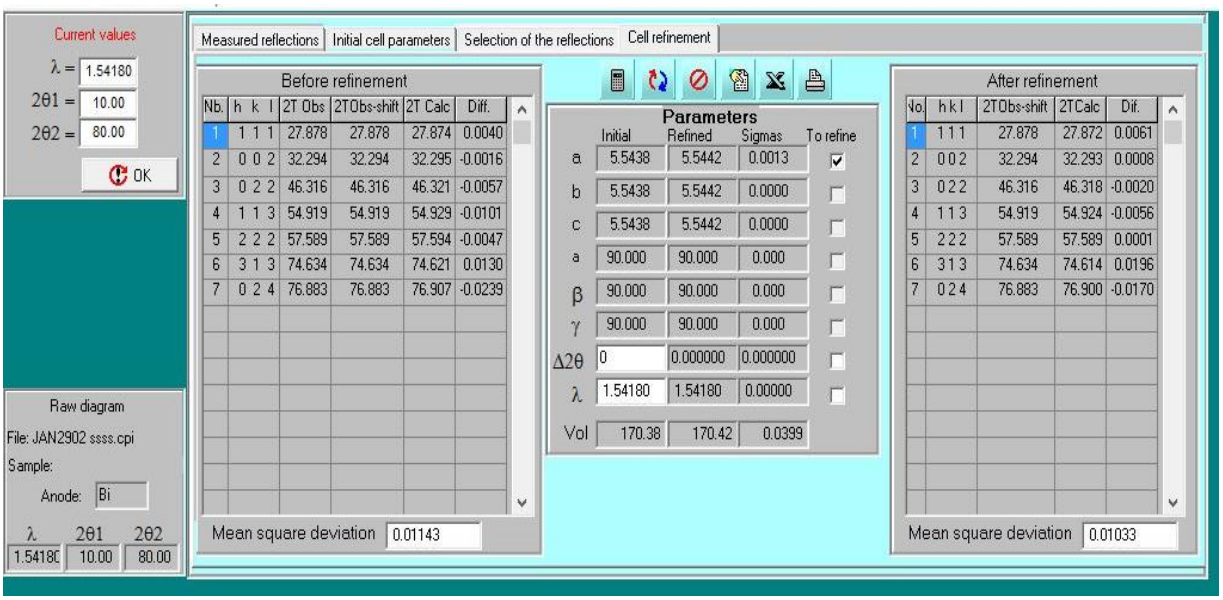

Fig14.: XRD data analysis by CELREF for BVO

The formation and structure of the compound can be confirmed by comparing the Bragg's position with the calculated one. Thus, it has been verified that CBO has tetragonal structure with space group tetragonal and space group P4/ncc and BVO has cubic structure with space group $Fm\bar{3}m$.

Table 6.: Samples and refined cell parameters

Samples	Phase	Cell parameters	Space Group	Unit cell Volume ($Å^3$)
CBO	Tetragonal	$a=b$=8.5009 Å c=5.8179 Å $\alpha=\beta=\gamma$=90°	P4/ncc	197.83
BVO	Cubic	$a=b=c$=5.5442 Å $\alpha=\beta=\gamma$=90°	$Fm\bar{3}m$	170.418

3.2 Energy band gap determination using UV-Visible Spectroscopy

The optical properties of the prepared samples were analyzed by UV-Visible absorption technique. To determine the direct optical band gap, Planck's equation was used.

$$E = \frac{hc}{\lambda}$$

Where h is Planck's constant, c is velocity of light and λ is wavelength.

Absorbance vs wavelength (nm) plots of CBO and BVO are as shown below.

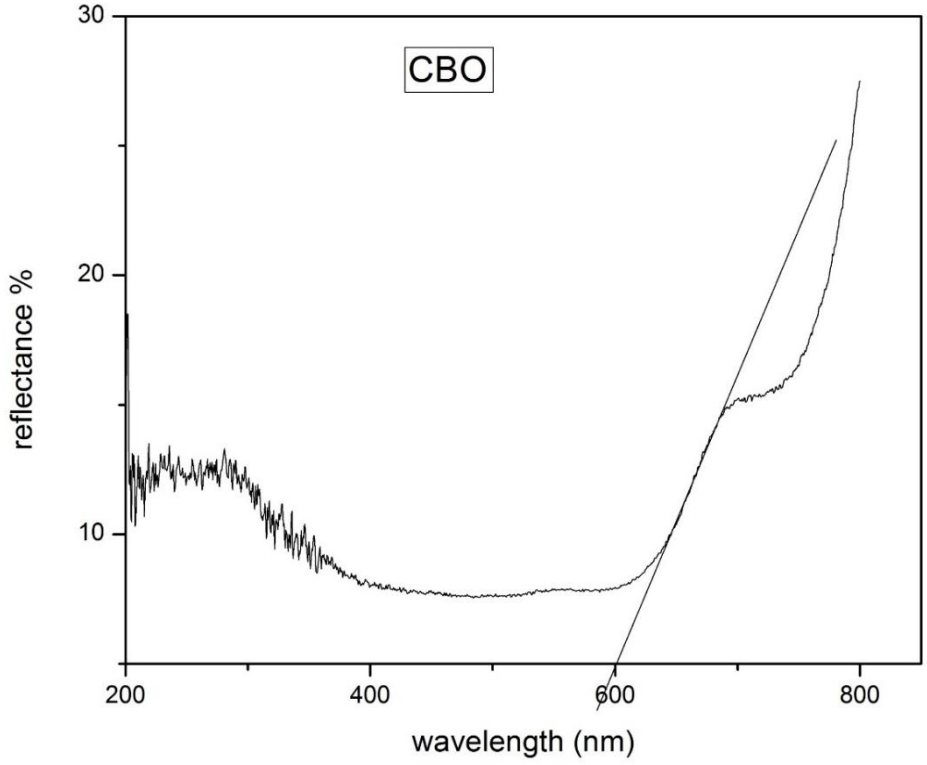

Fig 15.: Reflectance (%) vs wavelength (nm) plot for CBO

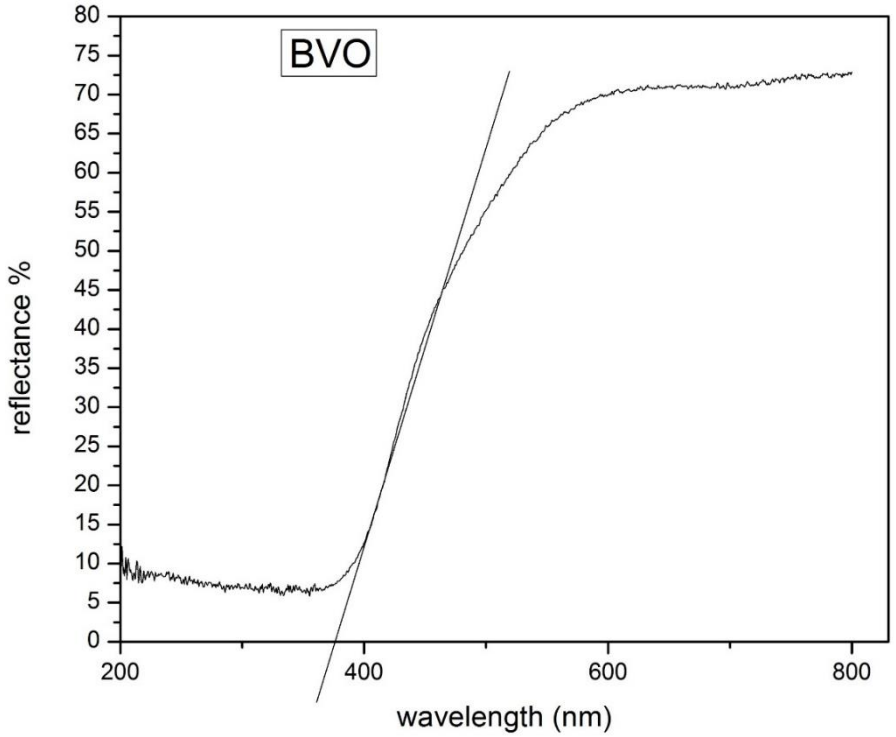

Fig 16.: Reflectance (%) vs wavelength (nm) plot for BVO

The band gap value as determined are presented in table:

Table 7: Optical band gap values of prepared samples

Sample	**Band Gap (E_g) (eV)**
$CuBi_2O_4$ (CBO)	2.07
$Bi_{0.913}V_{0.087}O_{1.587}$ (BVO)	3.314

The value of band gap of $CuBi_2O_4$ is 2.07 eV whereas the band gap of $Bi_{0.913}V_{0.087}O_{1.587}$ is 3.314 eV. The energy band gap value of $Bi_{0.913}V_{0.087}O_{1.587}$ determined in this study is higher than that of

a semiconductor, where gap value is ~1 eV. Therefore, it is reasonable to consider that the electronic conductivity will be negligible. The negligible electronic conduction property of $Bi_{0.913}V_{0.087}O_{1.587}$ sample meets the requirements of SOFC electrolytes.

3.3 Conductivity measurements

3.3.1 DC Conductivity of CBO

Conductivity of the sample was determined using a two probe method. Before conductivity measurement, cylindrical pellets of the sample were coated with commercial silver paste on top and bottom surfaces. This was done to provide proper electrical contact. The electrical conductivity was recorded as a function of temperature range of 50-500ºC based on two-probe method.

In order to determine conductivity of the sample, we measured the value of resistance *R* and substituted *R* in equation given below

$$\sigma = \frac{1}{R}\frac{l}{A}$$

Where *R* is resistance, *l* is thickness of pellet and *A* is the area of the sample

DC conductivity data of CBO sample is displayed in the form of conductivity (Scm^{-1}) v/s temperature(°C) plots [Fig. 17].

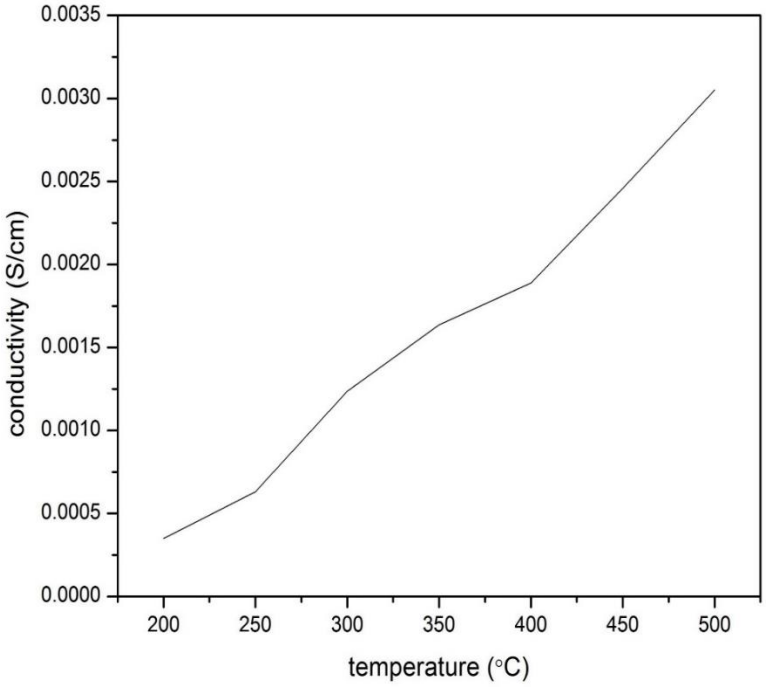

Fig. 17: DC conductivity plot for CBO at different temperatures

At low temperature the conductivity is low but at high temperature it is seen that conductivity increases exhibiting a semi conducting behaviour in the tested temperature range. It is noticed that an inflection occurred at around 400°C. This observation is generally consistent with the reported literature results N. Li et al. Hence, CBO is a pure electronic conductor below 400°C and possibly becomes a mixed ionic and electronic conductor due to dramatically increased ionic conductivity above 400°C. Therefore, the appearance of oxygen ionic conductivity above 400°C leads to a sharp increase in total electrical conductivity.

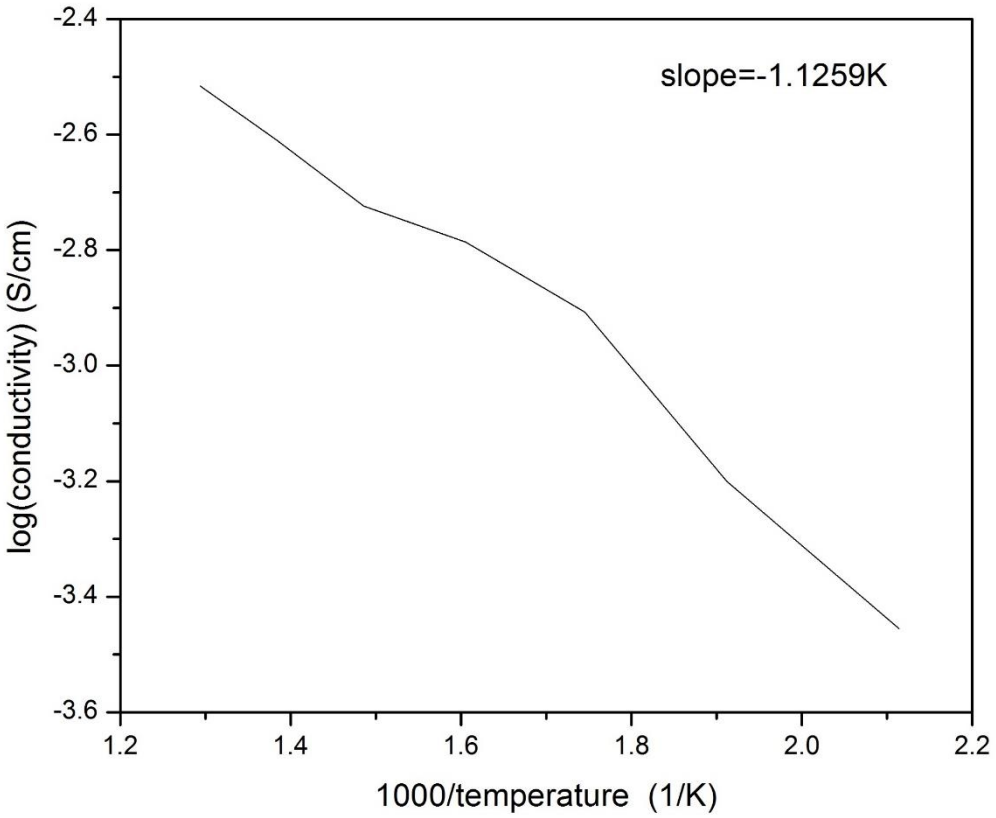

Fig.18: Arrhenius plot of the log(σ) vs 1000/T(K^{-1})

Fig. 18 shows the Arrhenius plot of the total electrical conductivity for CBO. The calculated activation energy E_a =9.4 J/mol. The E_a increases can be attributed to the rapid increase of oxygen iron conductivity above 400°C. It is generally believed that the E_a for ionic conduction is much larger than that for electronic conduction. Therefore, the increase of E_a value confirms the appearance of oxygen ion conduction at high temperature (above 400°C).

3.3.2 AC conductivity of BVO

Impedance spectroscopy technique was used to determine the conductivity of the $Bi_{0.913}V_{0.087}O_{1.587}$ sample. Before impedance measurement, cylindrical pellets of the sample were coated with commercial silver paste on top and bottom surfaces. This was done to provide electrical contact. Impedance data was recorded in the temperature range of 50-500ºC and in the frequency range of 1 Hz-10 MHz

Impedance data of $Bi_{0.913}V_{0.087}O_{1.587}$ is displayed in the form of Nyquist plots

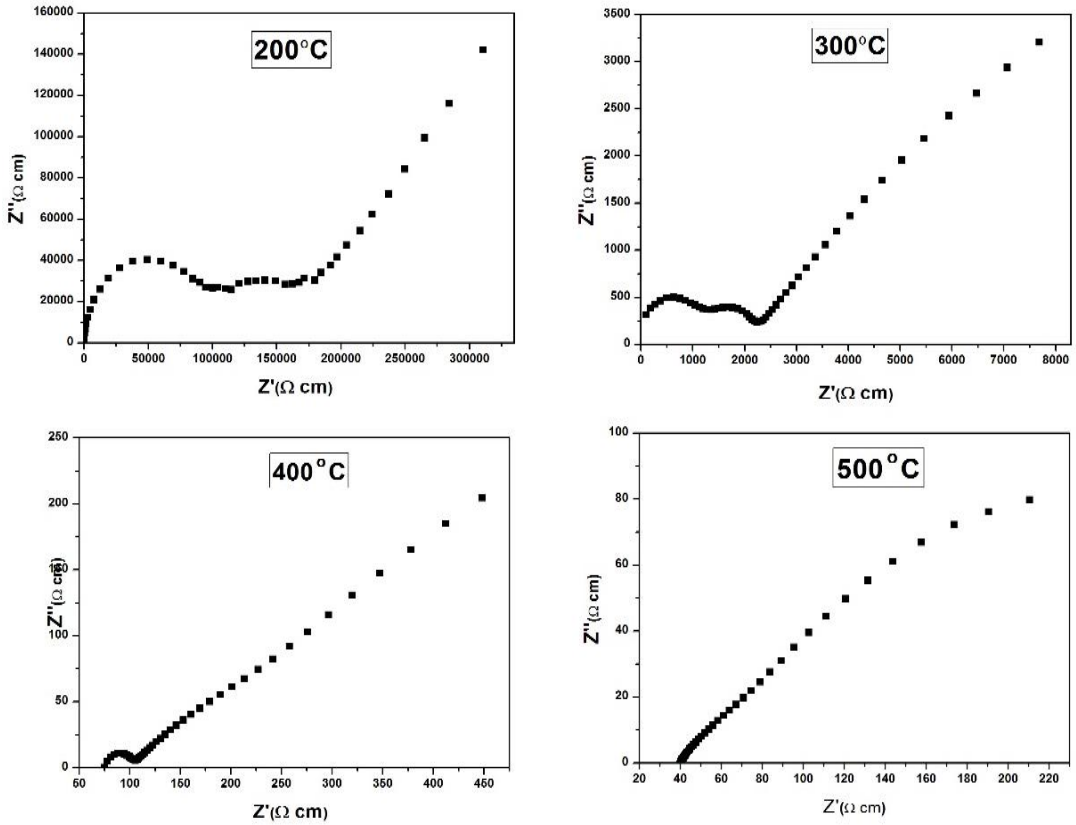

Fig 19: Complex impedance plane plot for $Bi_{0.913}V_{0.087}O_{1.587}$ at 4 different temperatures

At low temperatures, the Nyquist plots show two semicircles and a low-frequency spike due to grain, grain boundary and electrode-electrolyte interface resistances in the materials. However, a separate semicircle due to grain resistance was not observed in high temperatures. This is possibly due to very low grain capacitance. When temperature was increased further; the semicircle became smaller and shifted towards lower Z values, indicating a reduction of grain and grain boundary

resistance. The broadened semicircle observed at low temperature could be resolved into two semicircles as shown in figure. The capacitance of the high frequency semicircle has the value of the order ~10^{-12}F which is typical of the bulk component whereas the capacitance of the low frequency semicircle with value ~10^{-10} F is typical of grain boundary component. At higher temperatures, the predominant feature is a low-frequency spike inclined at the horizontal axis. It is a characteristic of ionic polarization phenomena occurring at the blocking electrodes, and thus supporting the idea that the conduction was predominantly ionic.

In order to determine conductivity for each composition of sample, we find the value of resistance R (R_g+R_{gb}) from the complex plane plots and substitute in equation given below

$$\sigma = \frac{1}{R}\frac{l}{A}$$

Where R is resistance, l is thickness of pellet and A is the area of the sample. The data of the total conductivity was used to plot the Arrhenius plot. Figure [19] shows the Arrhenius plot of conductivity for $Bi_{0.913}V_{0.087}O_{1.587}$.

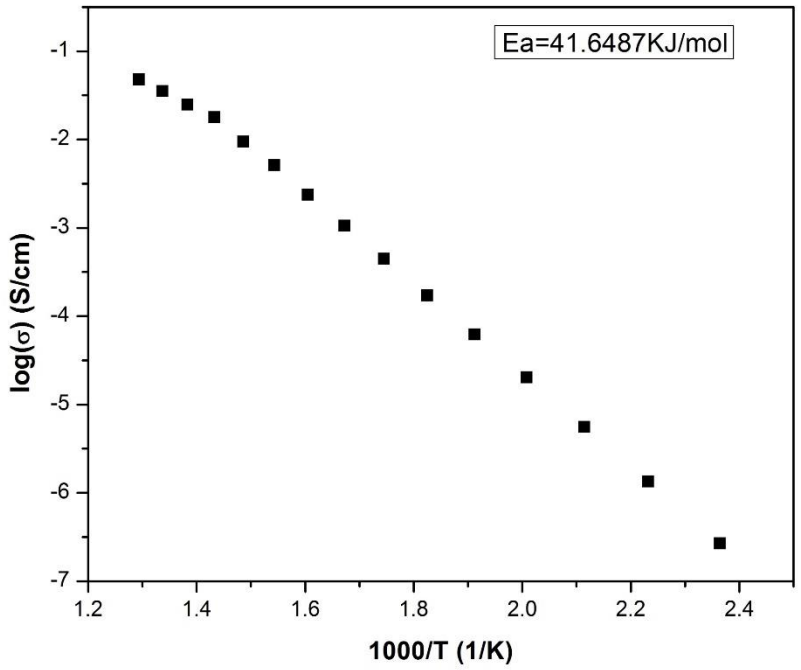

Fig.20: Arrhenius plot of conductivity for $Bi_{0.913}V_{0.087}O_{1.587}$

As can be seen from Arrhenius plot that there is a rise of conductivity above 400°C. The activation energy is high, Ea =41.6 KJ/mol which is desirable for ion conduction and hence low electronic conductivity.

Chemical stability of $CuBi_2O_4$ and $Bi_{0.913}V_{0.087}O_{1.587}$ mixture

$CuBi_2O_4$ and $Bi_{0.913}V_{0.087}O_{1.587}$ were mixed with 1:1 ratio to test their compatibility as cathode and electrolyte components in SOFC's. There is a possibility of phase formation by reaction of $CuBi_2O_4$ and $Bi_{0.913}V_{0.087}O_{1.587}$ at interface, thus reducing the ionic conductivity and the overall performance of the cell. Therefore, it is necessary to check the compatibility of the two components together.

0.25 g (1:1 ratio) of each $CuBi_2O_4$ and $Bi_{0.913}V_{0.087}O_{1.587}$ samples were mixed uniformly, heated at 400°C for 10 hours. X-ray diffraction pattern was obtained to check whether any extra peaks are observed. Fig. 21 Shows the XRD pattern of $CuBi_2O_4$, $Bi_{0.913}V_{0.087}O_{1.587}$ and mixture of both

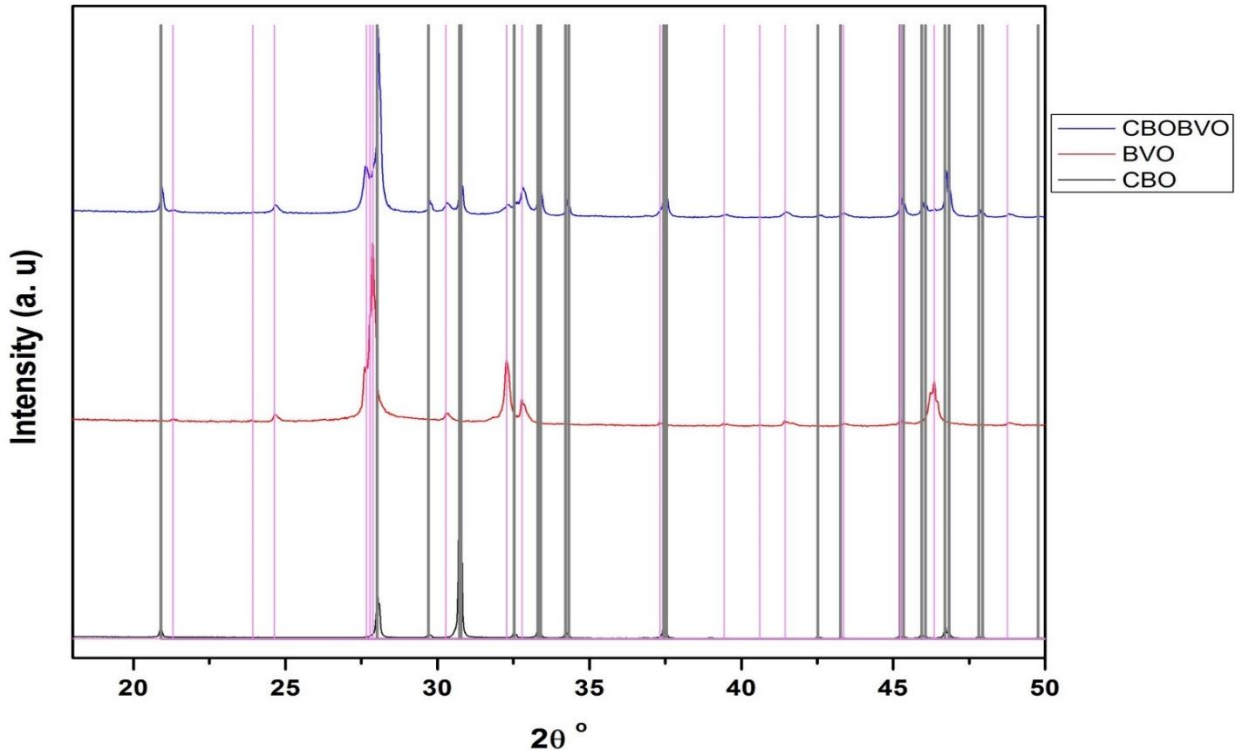

Fig. 21: XRD pattern of $CuBi_2O_4$, $Bi_{0.913}V_{0.087}O_{1.587}$ and mixture of both CBO and BVO.

CBO and BVO. It can be seen that all the diffraction peaks of (CBO+BVO) mixture match well with the XRD pattern of $CuBi_2O_4$ and $Bi_{0.913}V_{0.087}O_{1.587}$. No additional peaks were observed. This result imply that CBO and BVO both together qualifies as components of SOFC's.

CHAPTER 4

Conclusions & Future Scope

Conclusions:

- $CuBi_2O_4$ has Tetragonal structure with space group P4/ncc and has a high electronic conductivity below 400°C and above 400°C it exhibits electronic and ionic conductivity.
- $CuBi_2O_4$ has a low band gap value, 2.07eV and hence has a high electronic conductivity.
- $CuBi_2O_4$ is spinal compound with general formula $A_1B_2X_4$. X can be oxygen, selenium, sulphur, fluorine. A, B are metals with oxidation state +2 and +3 respectively. A metal belongs to group 2, d-block elements whereas B belongs to d block elements. A spinel unit cell is made up of 8 fcc cells. The anions occupy the fc lattice points. Anion X of the compound forms fc structure, hence there will be 8 tetrahedral voids and 4 octahedral voids in the spinel structure.

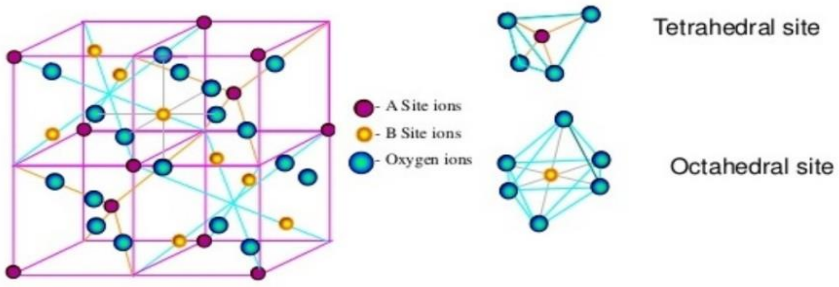

Fig. 22: A general spinel structure

- $Bi_{0.913}V_{0.087}O_{1.587}$ has cubic perovskite structure with space group $Fm\bar{3}m$. Additionally it has minor phase with space group I23 and has a high ionic conductivity below and low electronic conductivity.
- $Bi_{0.913}V_{0.087}O_{1.587}$ has a high band gap value, 3.314 eV and hence has a high ionic conductivity

- Is a perovskite compound. A perovskite is a material that has the same crystal structure as the mineral calcium titanium oxide, the first-discovered perovskite crystal. Generally, perovskite compounds have a chemical formula ABX_3, where 'A' and 'B' represent cations and X is an anion that bonds to both. A large number of different elements can be combined together to form perovskite structures. Using this compositional flexibility, scientists can design perovskite crystals to have a wide variety of physical, optical, and electrical characteristics. Perovskite crystals are found today in ultrasound machines, memory chips, and now – solar cells.

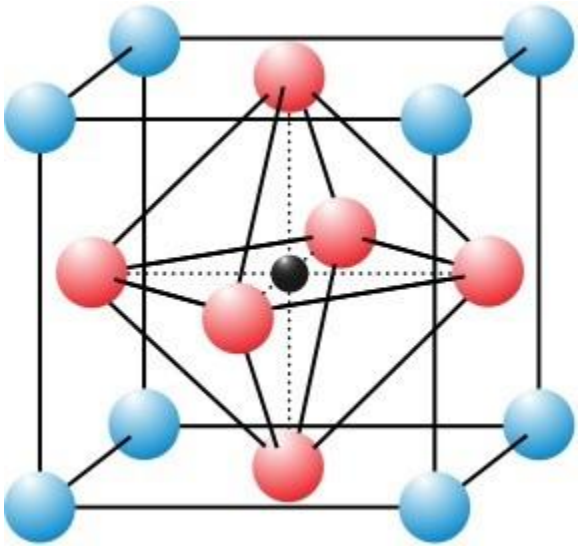

Fig. 23: Perovskite structure

- It is found that BVO and CBO qualify as electrolyte and cathode components for SOFC's and do not show any phase formation at 400°C.

Future Scope:

- Doping can be done with transition metal-ions to obtain maximum ionic conductivity.
- The ratio of oxygen vacancy and occupancy should be determined to find out the optimum condition for ion transports.
- Detailed structural studies are needed to understand the role of local and global structure on the ionic conduction property

References:

1) M. Lo. Faro *et al.,* "Intermediate temperature solid oxide fuel cell electrolytes", *Journal of the Indian Institute of Science,* **89:4** (2009) 363.

2) A. M. Azad *et al.,* "Bismuth oxide- based solid electrolytes for fuel cells", *Journal of material science.***29** (1994) 4135-4151.

3) (Yamada *et al*., 2002)

4) Wang Hay Kan *et al.,* "Trends in electrode development for next generation solid oxide fuel cells", *J. Mater. Chem. A,* **4** (2016) 17913–17932.

5) L. Malavasi *et al.,* "Oxide-ion and proton conducting electrolyte materials for clean energy applications: structural and mechanistic features", *Chem. Soc. Rev.,* **39,** (2010) ,4370

6) F. M. L. Figueiredo *et al.*"Electrolytes for solid oxide fuel cells", *WIREs Energy Environ2012. doi: 10.1002/wene.23*

7) Tatsumi Ishihara, "Materials for High-temperature Fuel cells" Wiley (2013).

8) A. Hooper, "Fast ionic conductors", *Contemporary Physics,* **19:2,** (1978) 147-168

9) Stephen J. Skinner *et al.,* "Oxygen ion conductors", *Materials today,***6** (2003) 30-37

10) Joseph R. Peet *et al.,* "Insight into Design of improved Oxide Ion Conductors: Dynamics and Conduction Mechanisms in $Bi_{0.913}V_{0.087}O_{1.587}$ solid electrolytes", *J. Am. Chem. Soc.*,**141**, (2019) 9989-9997

11) West A. R., "*Solid State Chemistry and its Applications"* John Wiley & Sons, Ltd (2014).

12) P. Shuk*et al.,* "Oxide ion conducting solid electrolytes based on Bi_2O_3", *Solid State Ionics,* **89** (1996) 179–196.

13) A. Laarif *et al.,* "The lone pair concept and the conductivity of bismuth Oxides Bi_2O_3"*Solid State Ionics*, **21** (1986) 183.

14) P.D Battle *et al.,* "Structural and dynamical studies of δ-Bi_2O_3 oxide ion conductors", *Journal of Solid State Chemistry*,**63** (1986) 8-15.

15) https://www.google.com/search?q=solid+phase+of+bi2O3&source=lnms&tbm=isch&sa=X&ved=2ahUKEwiA0anq49znAhUA7HMBHb03CcwQ_AUoAXoECA0QAw&biw=1422&bih=978#imgrc=aPQN7Rm8WgMnpM

16) https://www.google.com/search?q=http://www.chegg.comhomework.help/questions.and.answers/zirconium-dioxide-zro2-adopts-fluorite-crystal-shown-lattice-parameter-517&rlz=1C1CHBD_enIN819IN819&source=lnms&tbm=isch&sa=X&ved=2ahUKEwjwiprd5NznAhUa6nMBHQxCAoYQ_AUoAXoECAMQAw&biw=1422&bih=978#imgrc=tuk7DpTn7hj2GM

17) https://www.google.com/search?q=http%3A%2F%2Fwww.ikts.fraunhofer.de%2Fen%2Fdepartments%2Fenergy+bio-medical+technology%2Fmaterials+and+components%2Fsofc+stack.+development.html&tbm=isch&ved=2ahUKEwi21M2Y5tznAhXDSisKHZ42DesQ2-cCegQIABAA&oq=http%3A%2F%2Fwww.ikts.fraunhofer.de%2Fen%2Fdepartments%2Fenergy+bio-medical+technology%2Fmaterials+and+components%2Fsofc+stack.+development.html&gs_l=img.3...94787.97013..97887...0.0..4.248.875.0j4j1.....0....1..gws-wiz-img.....0.bFcfWOg7zUo&ei=ObxMXvbTGsOVrQGe7bTYDg&bih=979&biw=1403&rlz=1C1CHBD_enIN819IN819&hl=en#imgrc=BwIFD75-74pS-M

18) L. J. Gauckler *et al., "*Solid Oxide Fuel Cells: Systems and Materials*", Chimia,***58** (2004) 837-850

19) S.C. Singhal *, "Advances in solid oxide fuel cell technology", Solid State Ionics,***135,** Issue 1-4 (2000)305-313

20) https://www.doitpoms.ac.uk/tlplib/fuel-cells/sofc_electrode_materials.php

21) https://en.wikipedia.org/wiki/Bismuth(III)_oxide

22) Andrei A. Bunaciua *et al., "X-Ray Diffraction: Instrumentation and Applications", Critical Reviews in Analytical Chemistry*, 45:4 (2015) 289-299

23) West A. R., "*Solid State Chemistry and its Applications"* John Wiley & Sons, Ltd (2014), 239-241

24) Zhebo Chen and Thomas F. Jaramillo (n.d). *The Use of UV-visible Spectroscopy to Measure the Band Gap of a Semiconductor,* Department of Chemical Engineering, Stanford University Edited by Bruce Brunschwig 09/19/2017

25) Clark, B. J., Frost, T., & Russell, M. A. (1993*). UV Spectroscopy: Techniques, instrumentation and data handling.* London; New York: Chapman & Hall

26) Instrumentation and characterization Technique-Anna university, Chennai-shodhganga

27) Pankove, J. I., "*Optical process in semiconductors*", Prentice-Hall Inc., Englewood Cliffs, New Jersey, 1971, Ch-11.

28) Sze, S.M. & Kwok K. Ng., "*Physics of Semiconductor devices*" Wiley eastern Ltd., New Delhi (1979) p.52

29) https://en.wikipedia.org/wiki/Band_gap

30) https://eng.libretexts.org/Bookshelves/Materials_Science/Supplemental_Modules_(Materials_Science)/Insulators/Electrochemical_Impedance_Spectroscopy

31) J. T. S. Irvine et al., "*Electroceramics: Characterization by Impedance Spectroscopy", Adv. Mater*. **2** (1990) 132-134

32) Armstrong, R.D. and M. Todd. 1995. Interfacial electrochemistry. *In Solid State Electrochemistry*, ed. P.G. Bruce. Great Britain: Cambridge University Press.

33) Cogger, N. D., Evans, N. J. *An Introduction to Electrochemical Impedance Measurement*, 1999 Technical Note, Solartron Analytical Technical Report No. 6, Part No. BTR006, http://www.solartronanalytical.com/downloads/technotes/technote06.pdf

34) Reece, C., 2005. An Introduction to Electrochemical Impedance Spectroscopy (EIS). https://www.jlab.org/conferences/tfsrf/Thursday/Th_2_1-EISintroReece.pdf. Accessed March 27 2020

35) Gamry Instruments "Basics of Electrochemical Impedance Spectroscopy" Available online: https://www.gamry.com/application-notes/EIS/basics-of-electrochemical-impedance-spectroscopy/ Accessed on March 24 2020

36) Mario F. García-Sánchez *et al., "*An Elementary Picture of Dielectric Spectroscopy in Solids: Physical Basis*", Journal of Chemical Education,* **80** (2003) 1062.

37) Matthew T. Dunstan *et al.,* "Variable-Temperature Multinuclear Solid-State NMR Study of Oxide Ion Dynamics in Fluorite-Type Bismuth Vanadate and Phosphate Solid Electrolytes",*Chem. Mater*..**31** (2019) 1704-1714.

38) https://www.google.com/url?sa=i&url=https%3A%2F%2Fwww.researchgate.net%2Ffigure%2FSome-selected-materials-developed-as-cathode-for-an-SOFC-device-57_tbl2_319929257&psig=AOvVaw36nnVgeliZ6iL-nzyrWhuM&ust=1652518248508000&source=images&cd=vfe&ved=0CAwQjRxqFwoTCPDZ0LGM3PcCFQAAAAAdAAAAABAD

39) Electrode properties of $CuBi_2O_4$ spinel oxide as a new and potential cathode material for solid oxide fuel cells

40) Fuel cells: principles and applications by B Viswanathan & M Aulice Scibioh